Journal of Fluorescence
https://doi.org/10.1007/s10895-023-03512-9

RESEARCH

# Colorimetric Detection of $Cu^{2+}$ and $Ag^{+}$ Ions Using Multi-Responsive Schiff Base Chemosensor: A Versatile Approach for Environmental Monitoring

**Gasem Mohammad Abu-Taweel[1] · Hamed M. Al-Saidi[2] · Mubark Alshareef[3] · Mohsen A. M. Alhamami[4] · Jari S. Algethami[4,5] · Salman S. Alharthi[6]**

Received: 28 October 2023 / Accepted: 14 November 2023


## Abstract

In this study, we have synthesized a novel Schiff base-centered chemosensor, designated as **SB**, with the chemical name ((E)-1-(((6-methylbenzo[d]thiazol-2-yl) imino)methyl)naphthalen-2-ol). This chemosensor was structurally characterized by FT-IR, 1H NMR, UV-Vis and fluorescence spectroscopy. After structural characterization the chemosensor **SB** was subsequently employed for the detection of $Cu^{2+}$ and $Ag^{+}$, using fluorescence spectroscopy. The chemosensor **SB** showed excellent ability to recognize the target metal ions, leading to fluorescence enhancement and color change from yellow to yellowish orange for $Cu^{2+}$ and yellow to radish for $Ag^{+}$ ions. The detection capabilities of this chemosensor were impressive, showing excellent selectivity and an exceptionally low detection limit of 0.0016 μM for $Cu^{2+}$ and 0.00389 μM for $Ag^{+}$. Most notably, our approach enables the quantitative detection both metal ions in different water and soil samples at trace level. This achievement holds great promise for analytical applications and offers significant contributions to the field of chemical sensing and environmental protection.

**Keywords** UV-vis spectroscopy · Schiff base · FT-IR · Chemosensor · Metal ions

## Introduction

Heavy metals are a group of naturally occurring elements characterized by their high atomic weight and density [1]. While some of these metals play very important roles in different natural processes and human activities, their accumulation in the environment has raised major concerns due to their adverse effects on both human health and ecosystems [1–4]. The introduction of these metals into the environment occurs through both natural processes, such as weathering of rocks and volcanic activity, as well as anthropogenic activities, such as industrial processes, mining, waste disposal, agriculture processes and many others [5–8]. These metals can persist in the environment for extended periods due to their nondegradable nature, leading to their accumulation in water, soil, and air [9–11]. As a consequence, these metals cause serious environmental problems and have the potential to disrupt ecosystems and threaten human health, even at a trace level. The detrimental impact of heavy metals on the environment and living organisms is well-documented [3, 11–14]. Heavy metals can enter the food chain through processes such as bioaccumulation and biomagnification, which occur as metals are ingested by lower organisms and subsequently transferred to higher trophic levels. This accumulation can lead to significant health risks for humans and wildlife. In humans, exposure to heavy metals can have profound and deleterious effects on various organ systems. Acute heavy metal intoxication can lead to severe damage to vital organs such as the cardiovascular, gastrointestinal,

✉ Jari S. Algethami
Jsalgethami@nu.edu.sa

1 Department of Biology, College of Science, Jazan University, P.O. Box 2079, Jazan 45142, Saudi Arabia

2 Department of Chemistry, University College in Al-Jamoum, Umm Al-Qura University, 21955 Makkah, Saudi Arabia

3 Department of Chemistry, Faculty of Science, Umm Al-Qura University, 24230 Makkah, Saudi Arabia

4 Department of Chemistry, College of Science and Arts, Najran University, P.O. Box, 1988, 11001 Najran, Saudi Arabia

5 Advanced Materials and Nano-Research Centre (AMNRC), Najran University, 11001 Najran, Saudi Arabia

6 Department of Chemistry, College of Science, Taif University, P.O. Box 11099, Taif 21944, Saudi Arabia

and central nervous systems. Prolonged exposure to heavy metals, even in trace amounts, can result in chronic health issues, affecting various organs such as liver, kidneys, lungs, bones and endocrine glands [1, 4, 15–18]. Among these metals, $Cu^{2+}$ has attracted considerable attention due to their diverse roles in chemical, biological and industrial processes. Its distinctive properties, including its excellent malleability, conductivity, and corrosion resistance, have led to its extensive use in diverse applications ranging from electrical wiring and plumbing to electronics [4, 19–22]. In biological systems, $Cu^{2+}$ ions are essential to the proper functioning of proteins and enzymes involved in cellular processes. Enzymes such as superoxide dismutase, tyrosinase and cytochrome c oxidase depend on $Cu^{2+}$ ions for their catalytic activities. Additionally, $Cu^{2+}$ ions are essential for the development and maintenance of immune response modulation, iron metabolism regulation and connective tissues [23–26]. However, despite its essentiality, an excess amount of $Cu^{2+}$ ions can lead to toxic effects. Excessive $Cu^{2+}$ ions exposure can lead to cellular damage, oxidative stress, neurological disorders, and many other health issues [27–29]. On the other hand silver (Ag) has garnered substantial attention among various metals over recent decades. Renowned for its relatively soft nature, exceptional ductility, and malleability, silver stands as a premier transition metal that shows supreme thermal and electrical conductivity. This adaptability extends to its capacity to be molded into sheets or drawn into wires, rendering it invaluable across an extensive spectrum of applications. It has a wide range of applications in the electronics industry, catalysis, jewelry, long-life batteries, pharmaceuticals, mirror manufacturing, and aerospace applications [30, 31]. However, this widespread utility has many implications. Effluents containing $Ag^{+}$ ions, stemming from diverse applications, have found their way into the environment over the years, inducing various health concerns. Chronic exposure to $Ag^{+}$ ions has been linked to liver and kidney issues, argyrosis, skin and eye irritation, respiratory and intestinal tract effects, and alterations in blood cells. Enzymes can fall victim to their inactivation, as $Ag^{+}$ ions displace essential metal ions or bind to key functional groups, throwing biological systems into disarray [32–35]. Therefore, it is very important to develop highly sensitive and selective methods for the detection of these metal ions. Several techniques such as atomic absorption and emission spectroscopy, high-performance liquid chromatography, inductively coupled plasma spectrometry, anodic stripping voltammetry, capillary electrophoresis and many other techniques have been reported for the detection of these metal ions [36–44]. These methods have excellent selectivity and sensitivity but still suffer from certain limitations such as complicated operations, excessive sample pretreatment and expensive [45, 46]. Hence, the development of a sensitive, straightforward, cost-effective and selective methods to detect $Cu^{2+}$ and $Ag^{+}$ ions in diverse samples is very important. Among the various analytical techniques available, colorimetric and spectrofluorimetric methods stand out for their inherent simplicity, exceptional sensitivity, and remarkable selectivity. These techniques are instrumental in both quantitative and qualitative assessment of various metal ions and other pollutants without the need for expensive or sophisticated equipment. Over the years, numerous colorimetric and fluorescent chemosensors have been engineered to detect various metal ions, utilizing diverse sensing mechanisms. However, an ideal chemosensor must exhibit high selectivity and sensitivity towards the target analyte, water solubility, visible color change, and intense fluorescence. Schiff bases are indeed known for being relatively inexpensive, easy to synthesize and have excellent photophysical properties. These compounds containing N, O, and S atoms are particularly effective due to their strong coordinating abilities with various metal ions and give fluorescence signals, which could be used for the detection of various metal ions [47, 48]. In this study, we present the synthesis and characterization of a novel Schiff base-centered chemosensor ((E)-1-(((6-methylbenzo[d]thiazol-2-yl)imino)methyl) naphthalen-2-ol), and its application as a versatile tool for the colorimetric and fluorescence detection of $Cu^{2+}$ and $Ag^{+}$ ions in aqueous solutions. Through comprehensive spectroscopic analysis and mechanistic investigations, we demonstrate the remarkable selectivity and sensitivity of chemosensor towards these target metal ions. The visual color changes observed upon metal ion binding, combined with the precise analysis of absorption spectra, enable the quantification of these metal ions at trace levels. Our study highlights the potential of Schiff base chemosensors as valuable assets in the field of environmental monitoring and analytical chemistry, offering a versatile approach to addressing the challenges posed by heavy metal contamination.

## Experimental

### Materials and Methods

Methanol, ethanol, acetic acid, and distilled water were consistently employed throughout the experimental work. 2-amino-6-methyl benzothiazole, 2-hydroxy-1-nepthaldehyde, metal salts such as $Li^{+}$, $CuCl_2$, $MgCl_2$, $NiCl_2$, $MnCl_2$, $CoCl_2$, $AlCl_3$, $ZnCl_2$, $HgCl_2$, NaCl, $FeCl_3$, $CdCl_2$, $CrCl_3$, $AgNO_3$ and $Pb(acetate)_2$ were obtained from Sigma Aldrich. The FT-IR data was recorded using FT IR spectrophotometer (ABB MB3000) Japan. $^{1}H$ NMR spectra were obtained using a Varian INOVA 300 MHz spectrometer. For UV-Vis spectra analysis a Shimadzu UV/Visible spectrophotometer (UV-3600 plus) was used. Emission spectra of the chemosensor were recorded using the F-7000: Hitachi fluorescence spectrophotometer.

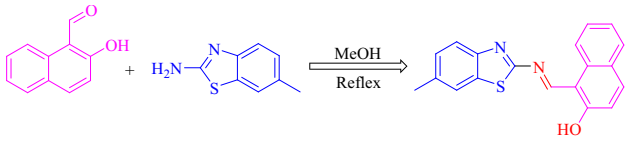


**Scheme 1** Synthesis of ((E)-1-((((6-methylbenzo[d]thiazol-2-yl)imino) methyl)naphthalen-2-ol)

## Synthesis of SB

**SB** was synthesized following the procedure described in the literature [49] as depicted in Scheme 1. 2-hydroxy-1-nepthaldehyde (1.0 mmol) was dissolved in 20 mL of methanol and a few drops of acetic acid were subsequently added, and the mixture was stirred vigorously for 20 minutes. A methanolic solution containing 2-amino-6-methyl benzothiazole (1.0 mmol) was then introduced, and the reaction was refluxed for 4 hours. The reaction progress was monitored with the help of thin-layer chromatography (TLC). Upon the completion of the reaction, the mixture was subsequently cooled to room temperature, resulting in the formation of yellow precipitates. These precipitates were isolated by filtration and washed several times with methanol. The resultant product was subjected to comprehensive characterization using modern spectroscopic techniques, including FT-IR, 1H-NMR, and UV-Vis spectroscopy (Figs. 1, 2 and 3). Yield: 92%; IR (KBr, $cm^{-1}$): 3400 (phenolic OH), 1617 (C=N imine group), 1549 (C=N thiazole group), 1315 (phenolic C-O), 818 (C-S-C); $^1$H-NMR (300 MHz, $CDCl_3$, δ, ppm): 2.482 (s, 3H, Methyl), 7.159 (d,1H, Hb, j = 9.604), 7.243 (s, 1H, Hi), 7.314(d, 1H, Hj, j = 8.644 Hz), 7.404 (t, 1H, He, j = 8.164 Hz), 7.623 (t, 1H, Hf, j = 7.683 Hz), 7.750 (d, 1H, Hd, j = 7.683 Hz), 7.859 (d, 1H, Hg, j = 8.644 Hz), 7.922 (d, 1H, Hi, j = 9.124 Hz), 8.316 (d, 1H, Hc, j = 9.604 Hz), 10.135 (s, 1H, CH=N), 14.423 (s, 1H, OH).

## General Procedure for Fluorescence Measurements

The sensing properties of **SB** were studied toward various cations such as $Mg^{2+}$, $Ni^{2+}$, $Co^{2+}$, $Ag^{+}$, $Al^{3+}$, $Zn^{2+}$, $Hg^{2+}$, $Na^{+}$, $Fe^{3+}$, $Cd^{2+}$, $Cr^{3+}$, $Pb^{2+}$, $Mn^{2+}$ and $Cu^{2+}$ ions. A 100 ppm stock solution of **SB** was prepared in methanol, while the above metal salts were dissolved in double-distilled water to prepare a 100 ppm solution. The stock solution of **SB** was subsequently diluted to prepare the working solution (10 ppm) in methanol: water (98:2 v/v) system. Different metal ion solutions were combined with **SB** in a 1:1 ratio within separate vials. The fluorescence titration experiments were conducted by transferring 2ml solution from each one stock solution into a quartz cuvette and the fluorescence spectra were recorded after a 10-minute interval in each instance. The chemosensor **SB** distinct response to $Cu^{2+}$ and $Ag^{+}$ ions was subjected to in-depth exploration encompassing aspects like pH effect, LOD,LOQ, stoichiometric ratio, selectivity and the effect of time. Furthermore, the developed chemosensor was applied for detecting $Cu^{2+}$ and $Ag^{+}$ invarious water samples, including tap, pond and river water. The titration experiments were carried out at room temperature.

## Samples Analysis

In order to assess the practical utility of the newly synthesized chemosensor **SB**, environmental samples (river water, tap water, pond water and soil samples) were subjected to analysis. These samples were spiked with a known quantity of $Cu^{2+}$ or $Ag^{+}$ ions and were subjected to triplicate experiments. The quantification of $Cu^{2+}$ and $Ag^{+}$ ions in these samples was conducted using the previously described procedure, and the percent recoveries were thoroughly investigated to gauge the accuracy of the method.

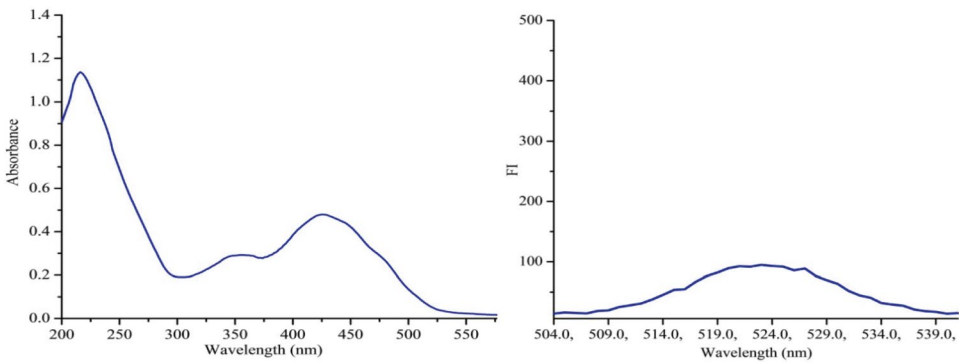


**a** UV-Vis spectra of **SB** (10 ppm) **b** Fluorescence spectra of **SB** (10 ppm)

**Fig. 1** **a** UV-Vis spectra of **SB** (10 ppm). **b** Fluorescence spectra of **SB** (10 ppm)

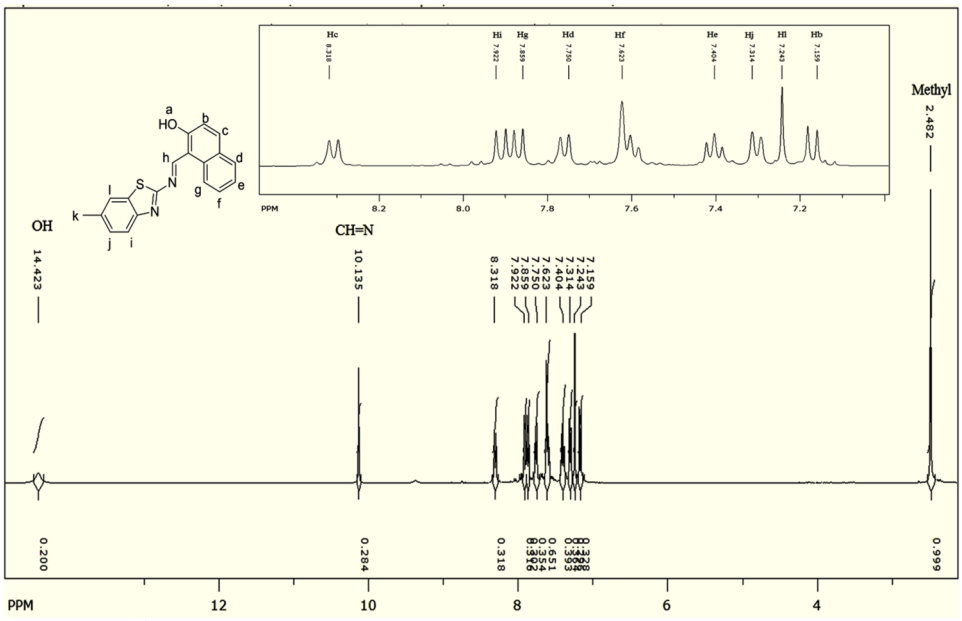


**Fig. 2** $^{1}$H NMR spectrum of ((E)-1-(((6-methylbenzo[d] thiazol-2-yl)imino)methyl) naphthalen-2-ol)

## Results and Discussion

### Characterization of SB

The chemosensor **SB** was subjected to comprehensive characterization using modern spectroscopic techniques, including UV-Vis, fluorescence, $^{1}$H-NMR and FT-IR (Figs. 1, 2 and 3). The UV–Vis absorption spectra ($\lambda_{max}$) for the free chemosensor **SB** was recorded in methanol:water (98:2 v/v) system at room temperature, with a concentration of 10 ppm. The spectra were recorded across a wavelength range from 200 to 600 nm. In the UV-Vis absorption

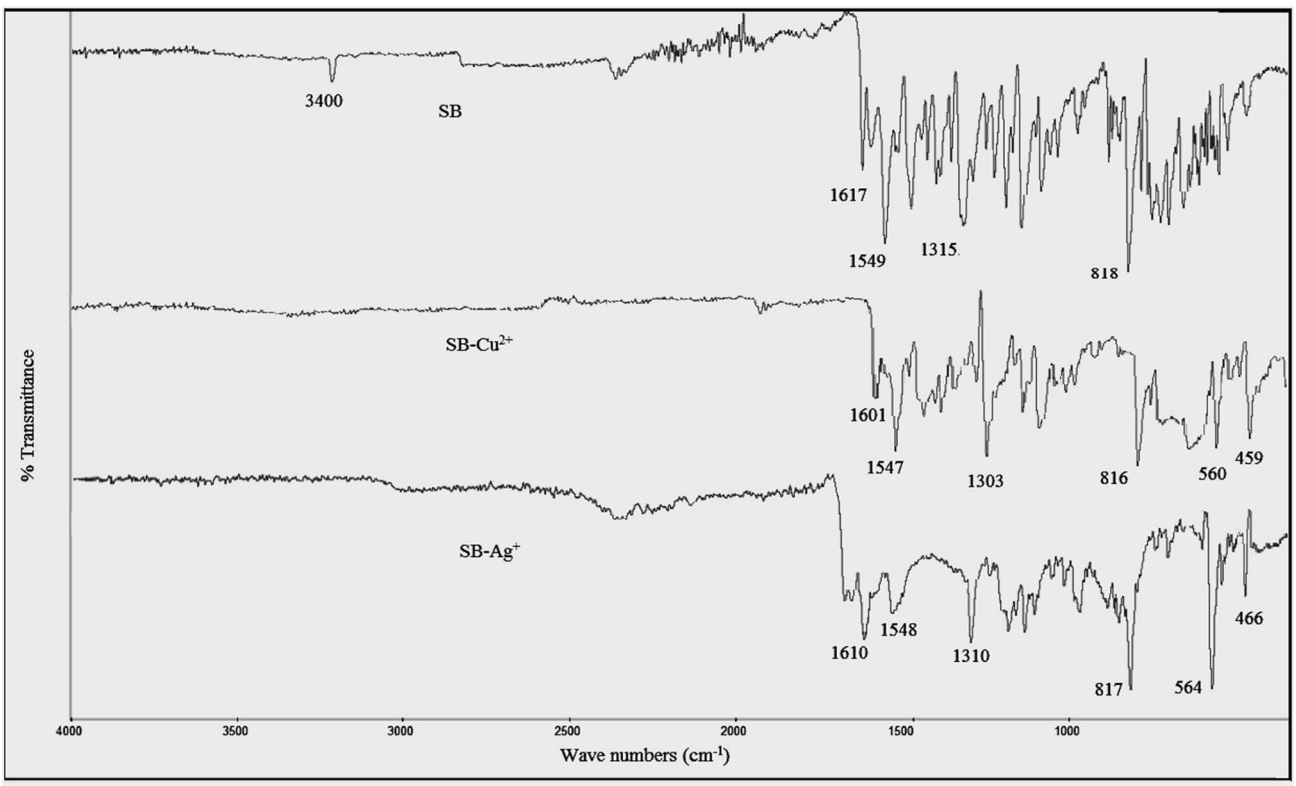


**Fig. 3** FT-IR spectraof **SB**, **SB**-$Cu^{2+}$ and **SB**-$Ag^{+}$

spectrum of **SB**, two distinct absorption peaks are prominently observed at 216 nm and 428nm, as depicted in Fig. 1a. These absorption bands hold significant implications as they are indicative of specific electronic transitions occurring within the molecule. The absorption peak centered at 216 nm is attributed to the π–π* transition. This transition involves the movement of an electron from a lower-energy π orbital to a higher-energy π* antibonding orbital. Such transitions typically occur in systems containing conjugated double bonds or aromatic rings, suggesting the presence of such structural motifs within **SB**. Conversely, the absorption peak at 428 nm is associated with the n–π* transition.

This transition involves the excitation of an electron from a non-bonding (n) orbital to a π* antibonding orbital. It is commonly observed in compounds containing electronegative atoms or groups, indicating the presence of imines and hydroxyl groups within the molecule [50]. The fluorescence spectra of the chemosensor was recorded at 523 nm when excited at 262 nm (Fig. 1b). The free chemosensor exhibited a relatively weak emission band at 523 nm. This weak emission photo-induced electron transfer (PET) from the N- atom imines group to naphthalene moiety. The $^{1}$H NMR spectra, highlighting distinct proton signals corresponding to specific parts of the molecule. Notably, a singlet peak at 2.482 ppm, signifies the presence of a methyl substituent. In the aromatic region, the spectrum reveals distinct peaks at 7.159 ppm, 7.243 ppm, 7.314 ppm, 7.404 ppm, 7.623 ppm, 7.750 ppm, 7.859 ppm, and 7.922 ppm, each representing different proton environments within the aromatic rings. Additionally, a singlet at 10.135 ppm confirms the presence of a CH=N group, while another singlet at 14.423 ppm indicates the presence of an -OH group (Fig. 2). Overall, the $^{1}$H-NMR spectrum provides precise information about the chemical shifts of protons in **SB**, facilitating the identification of the formation of the product.

## FT-IR of SB and SB-$Cu^{2+}$ and SB-$Ag^{+}$

The FT-IR peaks of **SB** and its $Cu^{2+}$ and $Ag^{+}$ complexes are presented in Fig. 3. Notably, the disappearance of specific FT-IR peaks associated with amino and carbonyl functional group provides compelling evidence for the formation of **SB**. Additionally, the emergence of new absorption peaks, particularly at 1617 $cm^{-1}$, is of significant importance. This specific band corresponds to the characteristic azomethine stretching vibration, confirming the condensation reaction between 2-hydroxy-1-nepthaldehyde and 2-amino-6-methyl benzothiazole. Additionally, the peak at 1549 $cm^{-1}$ is associated with the C=N stretching vibration of the thiazole ring, confirming the presence of this specific motif. The absorption peak at 1315 $cm^{-1}$ is indicative of the phenolic C-O stretching vibration. The appearance of absorption bands at 818 $cm^{-1}$, corresponding to ν(C-S-C). Furthermore, the absorption peak at 3400 $cm^{-1}$ is attributed to the phenolic hydroxyl (OH) group, indicating the presence of this moiety within the compound. In the complexes, a notable shift of the azomethine C=N band to lower frequencies by approximately 16 $cm^{-1}$ for $Cu^{2+}$ and 7 $cm^{-1}$ for $Ag^{+}$ was observed. This shift can be attributed to the withdrawal of electron density from the nitrogen atom. This change signifies the coordination of the C=N group to the metal ions. This phenomenon is indicative of the structural alteration upon complexation. Simultaneously, the peak observed at 1315 $cm^{-1}$ of **SB** due to C-O phenolic group, exhibited a shift towards lower frequencies by approximately 12 $cm^{-1}$ for $Cu^{2+}$ and 5 $cm^{-1}$ for $Ag^{+}$. This shift is consistent with the coordination of the phenolic oxygen to the metal ions within the complexes. The distinctive band attributed to –OH stretching vibrations at 3400 $cm^{-1}$ in the Schiff base was conspicuously absent in the complexes. This absence can be attributed to the deprotonation of the –OH group upon complexation, indicating the interaction of the phenolic oxygen with the metal ions. In the low-frequency region of the spectra, the complexes displayed new bands at 560 $cm^{-1}$ and 459 $cm^{-1}$ for the $Cu^{2+}$ complex, 564 $cm^{-1}$ and 466 $cm^{-1}$ for the $Ag^{+}$ complex. These bands were assigned to ν(M-O) and ν(M-N) stretching vibrations, respectively. This observation provides evidence for the presence of specific metal-oxygen and metal-nitrogen bonding interactions within the complexes. The ν(C-S-C) stretching vibration, which occurs at 818 $cm^{-1}$, and the ν(-C=N-) stretching vibration at 1549 $cm^{-1}$, remained practically unchanged in the complexes. This consistency supports the notion that the nitrogen and sulfur of the thiazole moiety are not directly involved with the metal ions [51–53].

## Naked Eye Colorimetric Detection of $Cu^{2+}$and $Ag^{+}$ Ions

The naked eye colorimetric studies were performed toward various cations such as $Li^{+}$, $Mg^{2+}$, $Ni^{2+}$, $Co^{2+}$, $Ag^{+}$, $Al^{3+}$, $Zn^{2+}$, $Hg^{2+}$, $Na^{+}$, $Fe^{3+}$, $Cd^{2+}$, $Cr^{3+}$, $Pb^{2+}$, $Mn^{2+}$ and $Cu^{2+}$ ions in a methanol:water (98:2 v/v) system at room temperature. Equimolar amounts of the aforementioned metal ions were separately introduced into the chemosensor solution. Significantly, the color of chemosensor solutions changes within a remarkably short reaction time of 1 minute upon the addition of respective metal ions. Notably, the color changes from yellow to yellowish orange for $Cu^{2+}$ and yellow to radish for $Ag^{+}$ ions (Fig. 4). This discernible alteration can be readily observed by the naked eye, exemplifying the simplicity and efficiency of the method. In Fig. 4, a digital photograph illustrates the evident color change in a solution containing chemosensor **SB** when introduced to

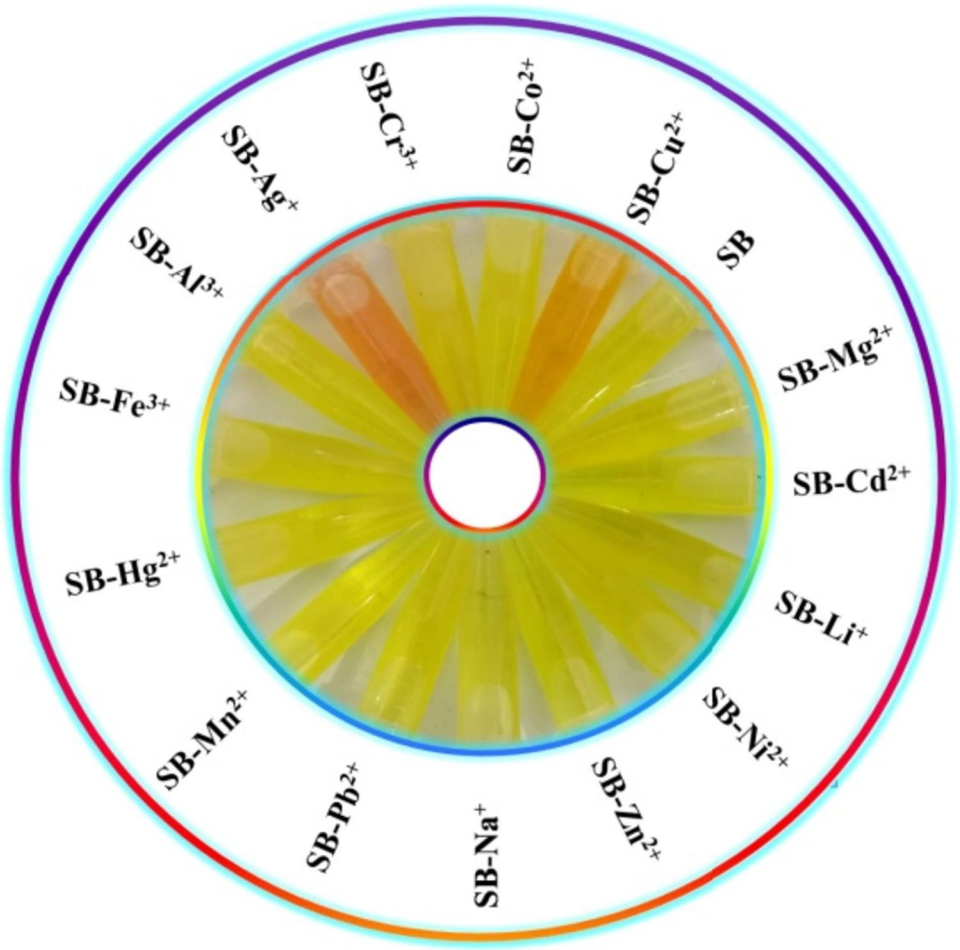


**Fig. 4** Colorimetric changes of chemosensor **SB**(10 ppm) in methanol: water (98:2 v/v) in the presence of 1equivalent of different metal ions

different metal ions. This straightforward visual distinction shows the method potential for sensitive and selective multi ions detection in aqueous environments.

## Sensing Properties of SB

To explore the sensing capabilities of chemosensor **SB**, absorption spectra were recorded for the chemosensor **SB** (10 ppm) in the presence of various metal ions at a concentration of 1 ppm. Various metal ions such as $Li^{+}$, $Mg^{2+}$, $Ni^{2+}$, $Co^{2+}$, $Ag^{+}$, $Al^{3+}$, $Zn^{2+}$, $Hg^{2+}$, $Na^{+}$, $Fe^{3+}$, $Cd^{2+}$, $Cr^{3+}$, $Pb^{2+}$, $Mn^{2+}$ and $Cu^{2+}$ ions were added to the chemosensor solution (methanol: water (98:2 v/v)) at room temperature to understand their impact on the absorption properties of chemosensor **SB**. The free chemosensor exhibited two distinct absorption peaks prominently observed at 216 nm and 428 nm, as depicted in Fig. 5. The absorption peak centered at 216 nm is attributed to the π–π* transition. Conversely, the absorption peak at 428 nm is associated with the n–π* transition. Remarkably, substantial changes were observed in the absorption properties of chemosensor **SB** upon interaction

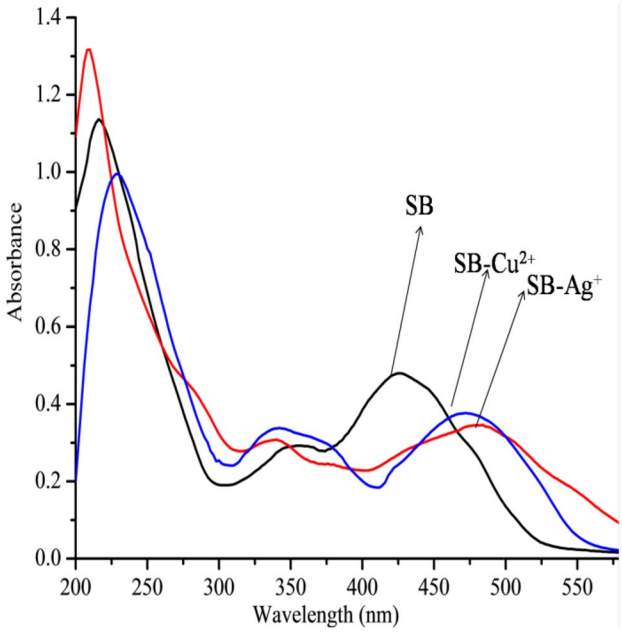


**Fig. 5** UV-Vis spectra of **SB** and its complexes with $Cu^{2+}$and $Ag^{+}$

with $Cu^{2+}$ or $Ag^{+}$ ions. The addition of $Cu^{2+}$ and $Ag^{+}$ ions induced noticeable changes, causing absorbance values to alter along with distinctive bathochromic spectral shifts of 44 and 60 nm, respectively, in the absorption spectrum of the chemosensor. This distinct bathochromic spectral shift in the absorption spectrum, specific to $Cu^{2+}$ and $Ag^{+}$ ions, not only differentiated them from other metal ions but also set them apart from each other. The changes in absorption properties, coupled with the observed color changes, strongly suggested significant interactions between the respective metal ions ($Cu^{2+}$ and $Ag^{+}$ ions) and functional groups, such as sulfur (C=N) and hydroxyl (-OH) groups, present in chemosensor.

The fluorescence characteristics of **SB** were also investigated toward $Li^{+}$, $Mg^{2+}$, $Ni^{2+}$, $Co^{2+}$, $Ag^{+}$, $Al^{3+}$, $Zn^{2+}$, $Hg^{2+}$, $Na^{+}$, $Fe^{3+}$, $Cd^{2+}$, $Cr^{3+}$, $Pb^{2+}$, $Mn^{2+}$ and $Cu^{2+}$ in methanol: water (98:2 v/v) system. The free chemosensor exhibited a relatively weak emission band at 523 nm when excited at 262 nm. This weak emission is due to PET from N- atom of imine group to naphthalene moiety. Upon the introduction of the above metal ions, a significant fluorescence enhancement was observed at 523 nm only for $Cu^{2+}$ and $Ag^{+}$ ions (Fig. 6). This fluorescence enhancement is due to the formation of complexes of **SB** with $Cu^{2+}$ and $Ag^{+}$ ions, which inhibit the PET effect. To gain further insights into $Cu^{2+}$ and $Ag^{+}$ ions sensing capabilities of **SB**, we conducted a titration experiment, gradually increasing the concentration of $Cu^{2+}$ and $Ag^{+}$ ions, (ranging from 0.005 to 1.00 ppm for $Cu^{2+}$ and 0.004 to 1.2 ppm for $Ag^{+}$ ) in a methanol: water (98:2 v/v) medium (Figs. 7 and 8).

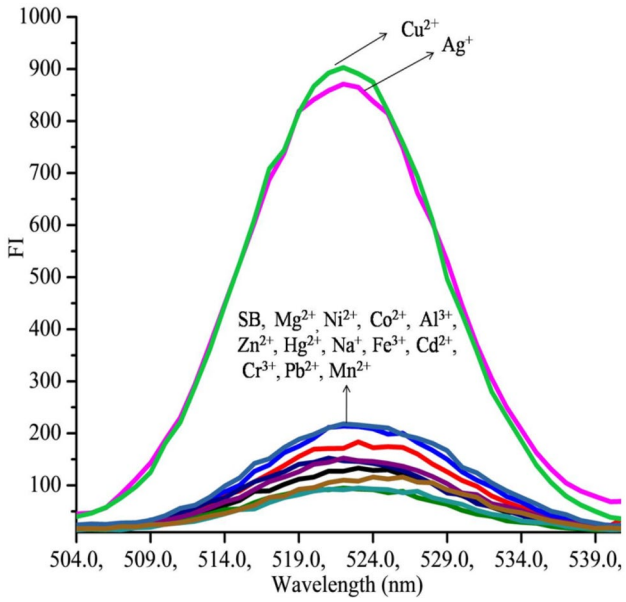


**Fig. 6** Fluorescence spectra of **SB** (10 ppm) in the presence of various metal ions (1 ppm)

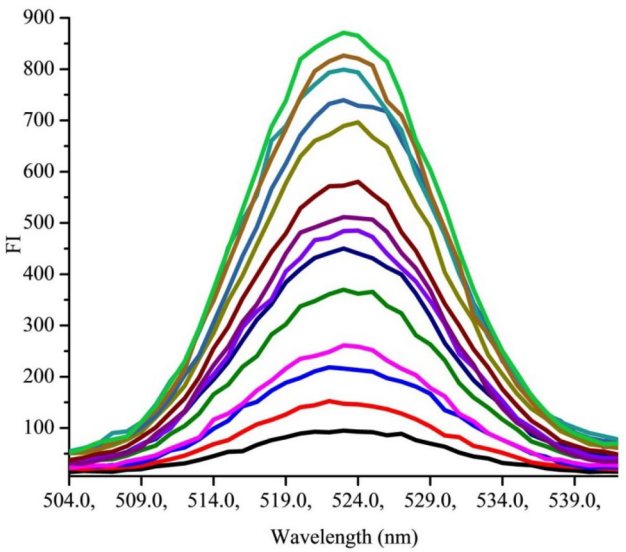


**Fig. 7** Fluorescence spectra of **SB** (10 ppm) with various concentration of $Ag^{+}$ (0.004-1.2 ppm)

The limit of detection (LOD) for $Cu^{2+}$ and $Ag^{+}$ ions were calculated as 0.0016 ppm (0.0251 μM) and 0.00389 ppm (0.0360 μM) respectively by using the formula: LOD = 3.3σ/S, and the limit of quantification (LOQ) was calculated as 0.00495 and 0.00389 μM, respectively by using the formula: LOD = 10/S, with the equation 10σ/S. Here, "σ" denotes the standard deviation, and "S" represents the slope of the curve obtained by plotting $F/F^{o}$ against the concentration of metal ions (Figs. 9 and 10).

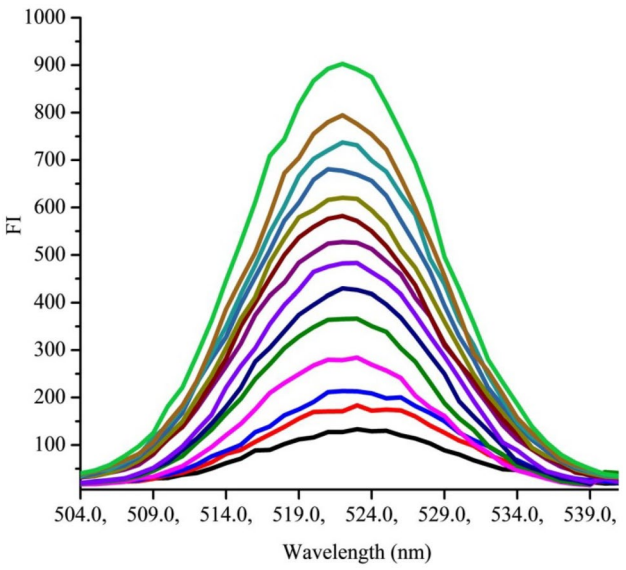


**Fig. 8** Fluorescence spectra of **SB** (10 ppm) with various concentration of $Cu^{2+}$ (0.005-1ppm)

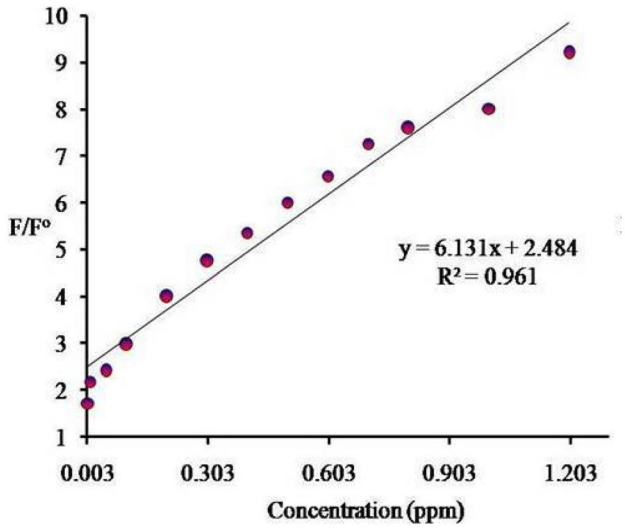


**Fig. 9** The plot of fluorescence spectra of **SB** (10 ppm) with various concentration of $Ag^+$ (0.004-1.2 ppm)

## pH Effect

The pH effect on the sensing applications of **SB** was studied with pH values ranging from 2 to 12. In separate test tubes, solutions at varying pH levels were prepared, each containing chemosensor **SB**, and their fluorescence intensity was measured. As depicted in Figs. 11 and 12, an interesting pH-dependent behavior was observed for the **SB-**$Cu^{2+}$ and **SB-**$Ag^+$ complexes. Notably, within the pH range of 2 to 6, very low enhancement was detected. This observation suggests

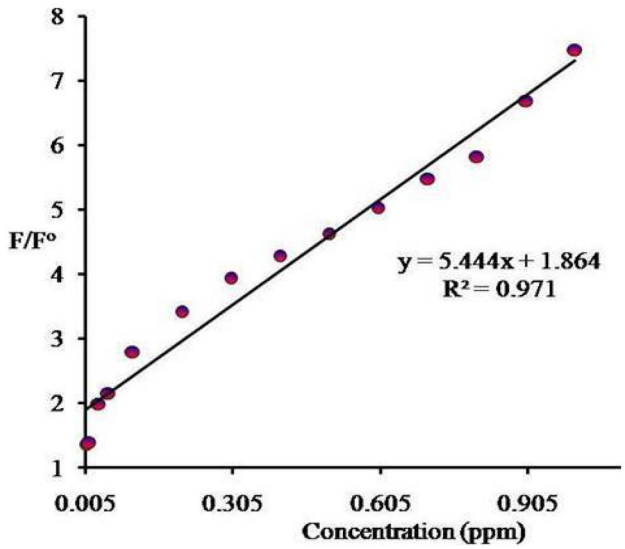


**Fig. 10** The plot of fluorescence of **SB** (10 ppm) with various concentration of $Cu^{2+}$ (0.005-1ppm)

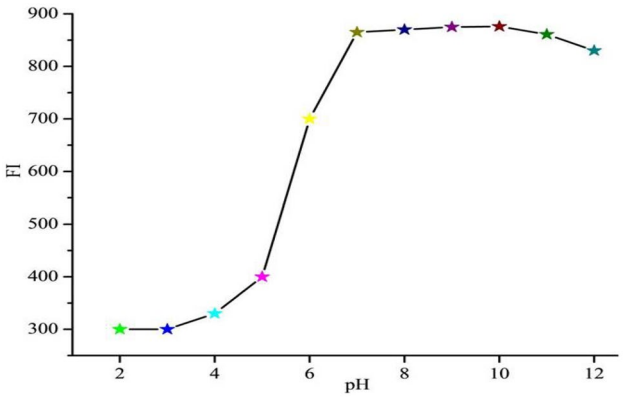


**Fig. 11** The effect of pH on the sensing response of **SB** toward $Ag^+$ ions

that the **SB-**$Cu^{2+}$ and **SB-**$Ag^+$ complexes do not form during this pH range. This phenomenon can be attributed to the protonation of -OH and -C=N- functional groups of **SB**, resulting in a reduction of its electron donation capability [54]. Consequently, the complexation between these metal ions and **SB** is hindered in this acidic pH range. However, as the pH increased from 7.0 to 11.0, a considerable increase in the fluorescence emission was observed at 523 nm, indicative of the formation of the **SB-**$Cu^{2+}$ and **SB-**$Ag^+$ complexes. This spectral change suggests that the interaction between the cations and **SB** becomes favorable as the solution becomes more neutral and basic. In this pH range, the deprotonation of relevant functional groups occurs, enhancing the electron donation ability and consequently leading to a stronger binding affinity between chemosensor and $Cu^{2+}$ and $Ag^+$ ions. The results conclusively indicate that the chemosensor **SB** can effectively serve as a detector for $Cu^{2+}$ and $Ag^+$ ions within the pH range of 7 to 11.

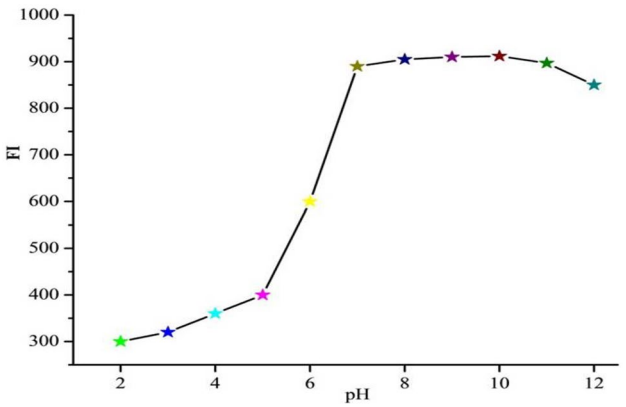


**Fig. 12** **The** effect of pH on the sensing response of **SB** toward $Cu^{2+}$ ions

## Time Effect

Time-dependent studies were conducted to investigate the impact of time on the stability of the SB-$Cu^{2+}$ and SB-$Ag^{+}$ complexes, with observations extending up to 50 minutes. The results revealed that the reaction between **SB** and metal ions ($Cu^{2+}$ and $Ag^{+}$) is remarkably fast. After dilution, consistent maximum fluorescence emission at 523 nm was rapidly achieved within just 10 minutes. This maximum absorbance remained constant and stable for the entire 50-minute duration of the experiment, as illustrated in Figs. 13 and 14. This observation indicates that the **SB-**$Cu^{2+}$ and **SB-**$Ag^{+}$ complexes form rapidly and exhibit excellent stability over an extended period, making them suitable for practical applications requiring prolonged detection or monitoring of $Cu^{2+}$ and $Ag^{+}$.

## Interference Experiments

In order to assess the practical utility of **SB** as an effective chemosensor for $Cu^{2+}$ and $Ag^{+}$ ions, interference experiments were conducted in the presence of other competitive coexisting metal ions. These experiments were carried out with 1 equivalent of various metal ions, such as $Li^{+}$, $Mg^{2+}$, $Ni^{2+}$, $Co^{2+}$, $Al^{3+}$, $Zn^{2+}$, $Hg^{2+}$, $Na^{+}$, $Fe^{3+}$, $Cd^{2+}$, $Cr^{3+}$, $Pb^{2+}$ and $Mn^{2+}$ ions. The results of these experiments revealed that the fluorescence intensity of **SB** by $Cu^{2+}$ and $Ag^{+}$ ions (1 equivalent each) remained unaffected in the presence of 1 equivalent of the other metal ions (Figs. 15 and 16). This observation suggests a strong interaction between chemosensor **SB** and $Cu^{2+}$ or $Ag^{+}$ ions in comparison to its interaction with other metal ions.

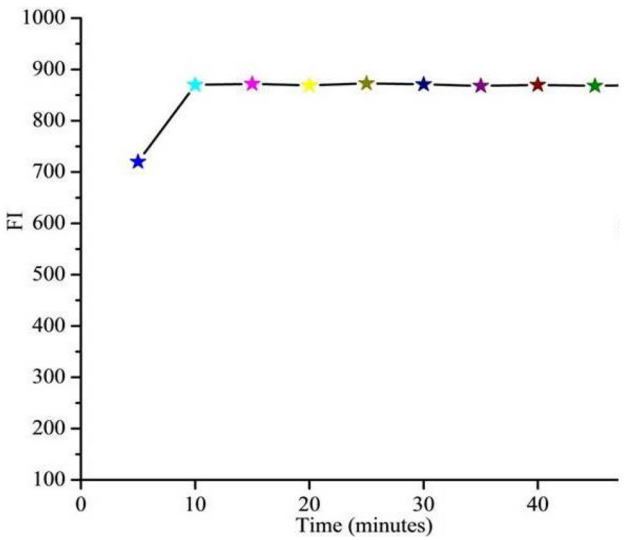


**Fig. 13** The effect of time on the stability of **SB**-$Ag^{+}$ complex

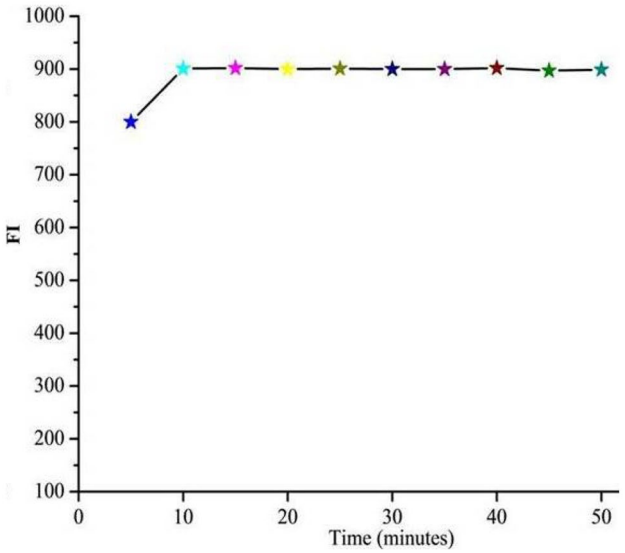


**Fig. 14** The effect of time on the stability of **SB**-$Cu^{2+}$ complex

## Job's Plot Analysis

The stoichiometric ration between chemosensor **SB** and $Cu^{2+}$ or $Ag^{+}$ ions investigated by Job's plot analysis using various volume ratios of chemosensor **SB** and $Cu^{2+}$ or $Ag^{+}$ ions (Figs. 17 and 18). The fluorescence intensity of **SB** at 523 nm was recorded against the molar fraction of $Ag^{+}$ or $Cu^{2+}$. Remarkably, in each case, the maximum fluorescence intensity was consistently reached at a molar fraction of 0.3. These findings provide compelling evidence supporting a 2:1 stoichiometric ratio between **SB** and $Ag^{+}$ or $Cu^{2+}$ ions.

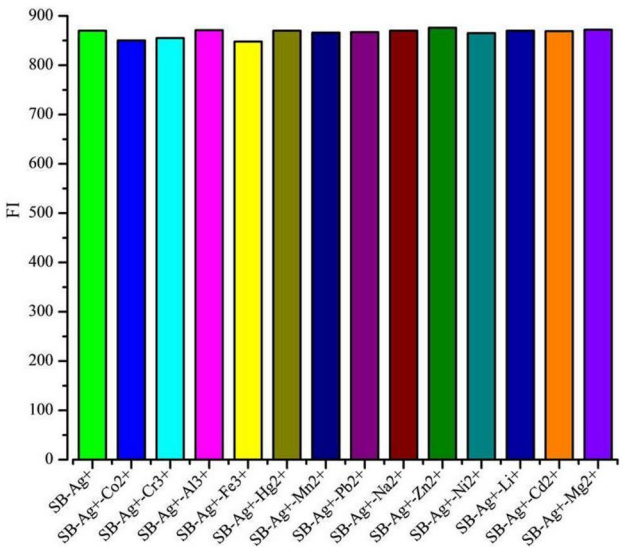


**Fig. 15** The effect various metal ions on the fluorescence intensity of **SB**-$Ag^{+}$ complex

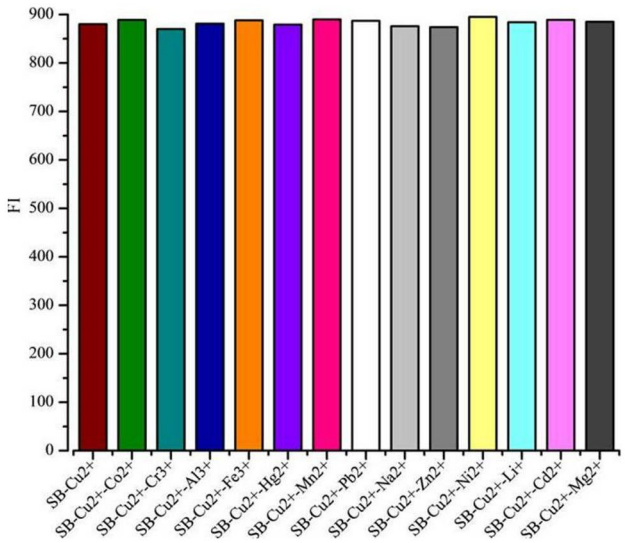


**Fig. 16** The effect various metal ions on the fluorescence intensity of **SB**-$Cu^{2+}$ complex

Scheme 2 presents the proposed mechanism depicting the formation of the **SB**-$Cu^{2+}$ and **SB**-$Ag^{+}$ complexes.

## Sensing Mechanism

The development of effective sensing mechanisms is very important for the detection and analysis of specific ions or molecules in various applications, ranging from environmental monitoring to biomedical diagnostics. The chemosensor **SB** has demonstrated remarkable capabilities in detecting and interacting with $Cu^{2+}$ and $Ag^{+}$. When these cations were introduced into the chemosensor solution, they formed chelating complexes (**SB**-$Cu^{2+}$ and **SB**-$Ag^{+}$).

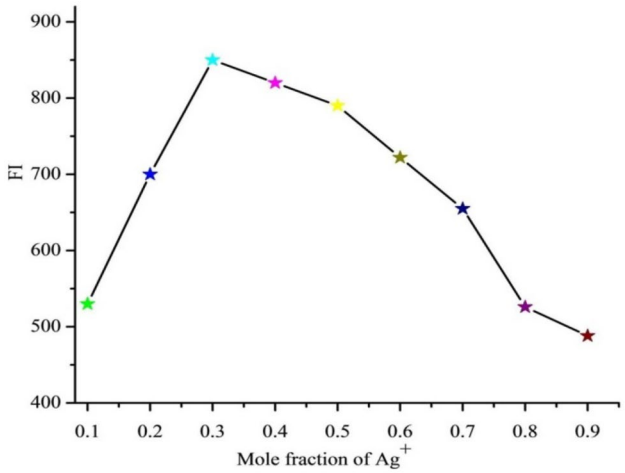


**Fig. 17** Job's plot of **SB** and $Ag^{+}$ in methanol: water (98:2 v/v) system

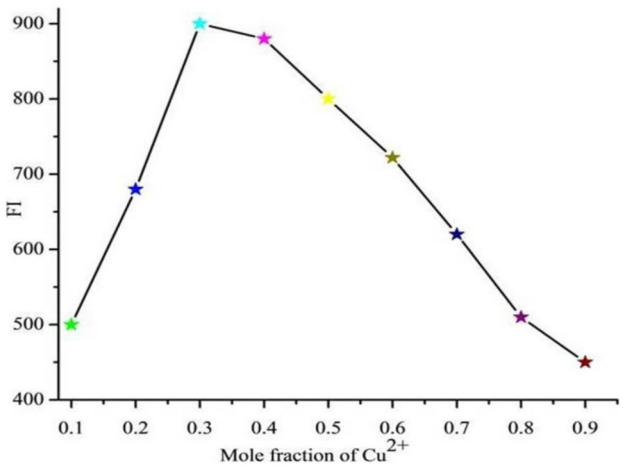


**Fig. 18** Job's plot of **SB** and $Cu^{2+}$ in methanol: water (98:2 v/v) system

The binding events primarily occur through the involvement of the phenolic oxygen and the nitrogen atom of the azomethine group (-CH=N-) (Scheme 2). These interactions represent pivotal steps in the sensing mechanism, leading to distinctive changes in the properties of **SB**. One of the notable alterations observed in the presence of $Cu^{2+}$ or $Ag^{+}$ is the pronounced color changes exhibited by **SB** in the presence of $Cu^{2+}$ or $Ag^{+}$ ions. The color of the chemosensor **SB** changes from yellow to yellowish orange for $Cu^{2+}$ and yellow to radish for $Ag^{+}$ ions. These color changes are reflective of the specific interactions occurring between **SB** and these metal ions.

Another intriguing aspect of the sensing mechanism is the appearance of red shifts of 44 nm for $Cu^{2+}$ and 60 nm for $Ag^{+}$ ions, which is a key indicator of the complex formation. This red shift can be attributed to two significant phenomena: ligand-to-metal charge transfer (LMCT) and the intramolecular charge transfer (ICT) effect. As these metal ions bind to the electron-donating groups of **SB** (O and N atoms), there is a reduction in the energy gap associated with the ICT band. This reduction results in the observed red shift in the absorption spectrum, providing spectroscopic evidence of complex formation. The fluorescence studies showed that the free chemosensor exhibited a relatively weak emission band at 523 nm due to the PET effect from the N-atom of imine group to the naphthalene moiety. Upon the introduction of $Cu^{2+}$ and $Ag^{+}$ ions, a significant fluorescence enhancement was observed at 523 nm. This fluorescence enhancement is due to the formation of complexes of **SB** with $Cu^{2+}$ and $Ag^{+}$ ions, which inhibit the PET effect.

To delve deeper into the binding stoichiometry between **SB** and $Cu^{2+}$ or $Ag^{+}$ ions, Job plot analysis was employed, which provides compelling evidence supporting a 2:1

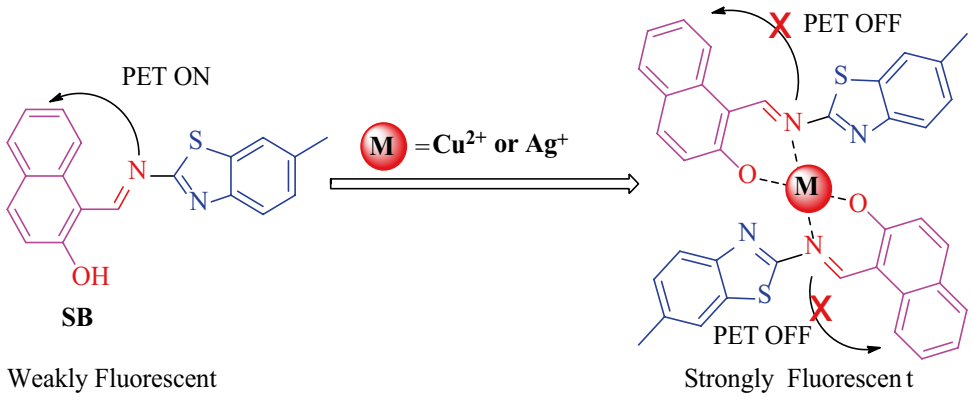


**Scheme 2** Possible sensing mechanism of the designed chemosensor **SB** for $Cu^{2+}$ or $Ag^{+}$

stoichiometric ratio between **SB** and $Ag^{+}$ or $Cu^{2+}$ ions. This finding elucidates the precise nature of the interactions, where two molecules of chemosensor **SB** coordinate with one ion of the respective metal. Spectroscopic evidence provides additional insights into the structural alterations induced by complex formation. Notably, a conspicuous IR shift in the azomethine C=N band to lower frequencies was observed in the complexes. This shift signifies the withdrawal of electron density from the nitrogen atom, highlighting the coordination of the C=N group with the metal ions. Simultaneously, the peak observed at 1315 $cm^{-1}$ of **SB** due to C-O phenolic group, exhibited a shift towards lower frequencies, also exhibited a shift towards lower frequencies. This shift aligns with the coordination of the phenolic oxygen to the metal ions within the complexes. Furthermore, the absence of the distinctive band attributed to -OH stretching vibrations at 3400 $cm^{-1}$ in the Schiff base of the complexes is indicative of the deprotonation of the -OH group upon complexation. This absence shows the interaction of the phenolic oxygen with the metal ions, revealing a significant structural change during complex formation. In the low-frequency region of the spectra, the complexes exhibited new bands at 564-560 $cm^{-1}$ and 466-459 $cm^{-1}$. These bands were assigned to $\nu$(M-O) and $\nu$(M-N) stretching vibrations, respectively. This spectral evidence offers concrete proof of the presence of metal-oxygen and metal-nitrogen bonding interactions within the complexes. Remarkably, certain key vibrational modes, such as the stretching vibration of (C-S-C) and (-C=N-) at 818 and 1549 $cm^{-1}$, respectively remained practically unchanged in the complexes. This consistency confirmed that nitrogen and sulfur of thiazole moiety are not directly involvedwith the metal ions. In conclusion, the sensing mechanism of chemosensor **SB** is a multifaceted process involving complexation with $Cu^{2+}$ and $Ag^{+}$ ions, resulting in distinct color, absorbance, and spectroscopic changes. These changes are supported by specific coordination interactions between **SB** and the metal ions, as evidenced by spectroscopic analysis and Job plot studies. This mechanistic understanding enhances the appreciation of **SB** as a versatile chemosensor for these metal ions.

## Comparison the Developed Chemosensor With Previously Reported Work

The sensing performance of the developed chemosensor **SB** was compared with reported chemosensors. It was observed that the chemosensor **SB** demonstrates notable advantages in terms of several parameters. One of the key strengths of the chemosensor **SB** is its remarkable sensitivity. When compared with similar chemosensors in the literature, the **SB** consistently exhibits higher sensitivity, allowing for the detection of even trace amounts of $Cu^{2+}$ and $Ag^{+}$ (Table. 1). Additionally, the chemosensor **SB** exceptional performance in an aqueous medium deserves special recognition. Aqueous environments are frequently encountered in various real-world applications, such as environmental monitoring and biomedical diagnostics, where maintaining chemosensor sensitivity and stability is challenging. The chemosensor **SB**, however, excels in such conditions, making it a highly promising choice for applications where the presence of water is a significant factor.

### Sensing Applications of SB

The chemosensor **SB** was applied for detecting $Cu^{2+}$ and $Ag^{+}$ in r river water, tap water, pond water and soil samples. The results, as summarized in Table 2, showed excellent recoveries ranging from 90% to 105%. These findings highlight the reliability and versatility of chemosensor **SB** in environmental and analytical chemistry, for the sensitive detection of $Cu^{2+}$and $Ag^{+}$ ions. This suggests that **SB** holds promise as a valuable tool for monitoring and assessing these ions in real-world samples.

**Table 1** Comparison of the performance of **SB** with various reported work for the detection of $Cu^{2+}$ and $Ag^{+}$

| Method | Analytes | Response | Color change | Mechanism | pH | LOD μM | Medium | References |
|---|---|---|---|---|---|---|---|---|
| Fluorimetric | $Cu^{2+}$ | On-Off | _ | ESIPT | 7.4 | 0.16 | Tris-HCl solution (70% THF) | [55] |
| Fluorimetric & Colorimetric | $Cu^{2+}$ | On-Off | Colorless to yellow | CHEQ | - | 2.14 | $CH_3CN$ | [56] |
| Fluorimetric & Colorimetric | $Ag^{+}$ | Turn-off | Yellow to orange | ICT | - | 10 | EtOH/$H_2O$ (1:1, v/v) | [57] |
| Fluorimetric | $Ag^{+}$ | Turn-on | - | ICT | 4-9 | 0.128 | MeOH/$H_2O$ (1:1,v/v) | [58] |
| Fluorimetric & Colorimetric | $Cu^{2+}$& $Pb^{2+}$ | Turn-on | Colorless to yellow | PET & ICT | 4.0–12.0 | 1.2 | CH3OH–tris-buffer (1: 1, v/v) | [59] |
| Fluorimetric | $Cu^{2+}$ | Turn-of | - | CHEQ | 6.0–12 | 0.69 | HEPES buffer solution (10 mM) | [60] |
| Fluorimetric | $Ag^{+}$, $Fe^{3+}$ | Turn off | - | Chelation | 4-13 | 0.423 | THF/$H_2O$, v/v, 1/1) | [61] |
| Fluorimetric | $Ag^{+}$ | Turn-on | - | ILCT | 7.21 | 6.20 | CH3CN:H2O (1:1, v/v) | [62] |
| Fluorimetric | $Cu^{2+}$ | Turn-off | - | CHEQ | 7 | 0.0901 | HEPES buffer at pH 7.0 ± 0.2 | [63] |
| Fluorimetric & Colorimetric | $Ag^{+}$ | Turn-on | - | Chelation | - | 0.12 | Ethanol | [64] |
| Fluorimetric & Colorimetric | $Cu^{2+}$ | Turn-on | Colorless to reddish pink | ICT, CHEF & PET | 7.4 | 0.0422 | CH3CN/H2O (1:1, v/v) | [65] |
| Fluorimetric & Colorimetric | $Ag^{+}$ | Turn-off | Colorless to orange | Chelation | 3–10 | 63.7 | DMSO/H2O (1/1, v/v) | [66] |
| Fluorimetric | $Cu^{2+}$ & $Co^{2+}$ | Turn-on | - | PET and LMCT | - | 1.98 | $CH_3CN$ | [67] |
| Fluorimetric | $Ag^{+}$ | Turn-on | - | PET | - | 3.15 | DMSO | [68] |
| Fluorimetric & Colorimetric | $Cu^{2+}$ | Turn-on | Yellow to yellowish brown | PET & CHEF | 7.0–10.0 | 0.03934 | MeOH/Water (10/90, v/v) | [69] |
| Fluorimetric | $Ag^{+}$ | Turn off | - | CHEF | 6-9 | 0.44 | MeOH-$H_2O$ (v/v=1:1) | [70] |
| Fluorimetric & Colorimetric | $Cu^{2}$ | Turn-on | Light yellow to light green | ICT & CHEF | 6–8 | 0.6 | MeOH–$H_2O$ (7:3) | [71] |
| Fluorimetric | $Ag^{+}$ | - | Colorless to black | Chelation | - | 1.0 | Methanol–tris-HCl buffer (1: 1) | [72] |
| Fluorimetric & Colorimetric | $Ag^{+}$, $I^{-}$ | Turn-off | Greenish yellow to colorless | ICT | 7 | 1.36 | DMSO: Water (1:1, v/v) | [73] |
| Fluorimetric & Colorimetric | $Cu^{2+}$ | Turn-off | Colorless to yellow | CHEQ | 7.0 | 1.49 | $CH_3CN$/$H_2O$ (95/5%) | [74] |
| Fluorimetric & Colorimetric | $Cu^{2+}$ | Turn-off | Light yellow to light brown | CHEQ | 7.0 | 3.0 | DMSO/H2O (1:1, v/v) | [75] |
| Fluorimetric & Colorimetric | $Ag^{+}$ | Turn-on | yellow to colorless | PET | 7.4 | 0.279 | Ethanol/water (1:9 v/v) 1:1 | [76] |
| Fluorimetric & Colorimetric | $Ag^{+}$ | Turn-off | Green to brown red | Chelation | - | 0.5 | THF | [77] |
| Fluorimetric | $Cu^{2+}$ | Turn-off | Yellow to wine red | ICT & CHEQ | 7.54 | 0.04 | DMF | [78] |
| Fluorimetric | $Ag^{+}$ | Turn-on | - | ICT | 7–13 | 5 | $H_2O$/MeOH (1 : 1 v/v) | [79] |
| Fluorimetric | $Cu^{2+}$ | turn-off | - | PET | 7.0 | 0.64 | $H_2O$/MeOH (1:1, v/v). | [80] |
| Fluorimetric | $Ag^{+}$ | Turn-on | - | PET,ICT | 5–8 | 0.15 | MeOH/H2O (1:1 (v/v) | [81] |
| Fluorimetric & Colorimetric | $Cu^{2+}$ | Turn-off | Yellow to pale-yellow | ICT & LMCT | 6.0 -13.0 | 0.179 | DMSO/$H_2O$ (1:3, V/V) | [82] |

**Table 1** (continued)

| Method | Analytes | Response | Color change | Mechanism | pH | LOD µM | Medium | References |
|---|---|---|---|---|---|---|---|---|
| Fluorimetric | $Ag^{+}$ | Off-on | - | ICT | 7.4 | 14 | MeOH-H2O (1:1, v/v) | [83] |
| Fluorimetric & Colorimetric | $Cu^{2+}$ | Turn-off | Colorless to yellow | CHEQ | - | 0.046 | Methanol | [84] |
| Colorimetric | $Cu^{2+}$ | - | Colorless to pink | Ring opening | - | 0.51 | THF | [85] |
| Fluorimetric & Colorimetric | $Ag^{+}$ | On−off | Yellow to shallow orange | ICT | - | 0.325 | DMSO/$H_2O$ (6:4, v/v) | [86] |
| Colorimetric& Fluorometric | $Cu^{2+}$ | Turn-on | Orange to yellow-green | PET | 6 | 0.713 | $CH_3CN/H_2O$ (3:7, v/v) | [87] |
| Fluorimetric & Colorimetric | $Cu^{2+}$ | Turn-on | Yellow to yellowish orange | PET | 7-11 | 0.0251 | Methanol: water (98:2 v/v) | Present work |
| Fluorimetric & Colorimetric | $Ag^{+}$ | Turn-on | Yellow to radish | PET | 7-11 | 0.0360 | Methanol: water (98:2 v/v) | Present work |

**Table 2** % Recovery of $Cu^{2+}$ and $Ag^{+}$ form river, tap and pond water samples

| Samples | Concentration of $Cu^{2+}$ (µg $mL^{-1}$) | | % Recovery | Concentration of $Ag^{+}$ (µg $mL^{-1}$) | | % Recovery |
|---|---|---|---|---|---|---|
| | Added | Found | | Added | Found | |
| River water | 1 | 0.9 | 90 ± 0.28 | 1 | 0.935 | 93.3. ± 0.45 |
| | 1.5 | 1.41 | 94 ± 0.30 | 1.5 | 1.46 | 97.3 ± 0.53 |
| | 3 | 2.95 | 98.3 ± 0.39 | 3 | 3.15 | 105 ±0.61 |
| Tap water | 1 | 0.94 | 94 ± 0.33 | 1 | 0.95 | 95 ±0.17 |
| | 1.5 | 1.46 | 97.3 ± 0.41 | 1.5 | 1.48 | 98 ± 0.32 |
| | 3 | 3.1 | 103.3 ± 0.47 | 3 | 3.08 | 102.6 ±0.35 |
| Pond water | 1 | 0.914 | 91.4 ± 0.19 | 1 | 0.97 | 97 ± 0.25 |
| | 1.5 | 1.49 | 99.3 ± 0.30 | 1.5 | 1.52 | 101.3 ± 0.31 |
| | 3 | 3.15 | 105 ± 0.39 | 3 | 3.14 | 104.6 ± 0.39 |
| Soil | 1 | 0.94 | 94 ± 0.14 | 1 | 0.95 | 95 ± 0.22 |
| | 1.5 | 1.48 | 98.6 ± 0.27 | 1.5 | 1.49 | 99.33 ± 0.34 |
| | 3 | 2.98 | 99.33 ± 0.35 | 3 | 3.08 | 102.6 ± 0.39 |

## Conclusion

In this work we synthesized a novel Schiff base chemosensor **SB** and characterized by various spectroscopic techniques, including FT-IR, 1H NMR, and UV-Vis spectroscopy, to verify its structural properties. The sensing properties of chemosensor were investigated toward different metal ions. Among the tested metal ions, **SB** demonstrated exceptional selectivity and sensitivity toward $Cu^{2+}$ and $Ag^{+}$. Notably, this chemosensor facilitated rapid, observable color changes visible to the naked eye upon interaction with these target metal ions. One of the most striking features of **SB** was its impressively low detection limit, highlighting its potential to detect trace levels of $Cu^{2+}$ and $Ag^{+}$ ions. The mechanism underlying the change in color and fluorescence emission of **SB** involved the coordination of metal ions with the nitrogen and oxygen atoms within the chemosensor. This coordination blocks the PET process which changes its photophysical properties and serves as the basis for detection. Our approach offers quantitative determination of these metal ions in river water, tap water, pond water and soil samples. The results showed excellent recoveries ranging from 90% to 105%. These findings highlight the reliability and versatility of chemosensor **SB** in environmental and analytical chemistry, for the sensitive detection of $Cu^{2+}$ and $Ag^{+}$ ions.

**Acknowledgements** The authors are thankful to the Deanship of Scientific Research at Najran University for funding this work, under the Research Groups Funding program grant code (NU/RG/SERC/12/5).

**Authors' Contributions** Gasem Mohammad Abu-Taweel: Writing Original Draft-Equal, Conceptualization-Equal, Hamed M. Al-Saidi: Data Curation-Equal, Formal analysis-Equal, Mubark Alshareef: Visualization-Equal, Editing-Equal, Mohsen A. M. Alhamami: Data Curation-Equal, Conceptualization-Equal, Jari S. Algethami: Supervision-Equal, Editing-Equal, Salman S. Alharthi: Data Curation-Equal, Editing-Equal.

**Funding** This research was funded by the Deanship of Scientific Research at Najran University, grant code (NU/RG/SERC/12/5).

**Data Availability** All data generated or analyzed during this study are included in this published article.

**Code Availability** Chem Draw.

## Declarations

**Ethical Approval** This article does not contain any studies with human participants or animals, clinical trial registration, or plant reproducibility performed by any authors.

**Consent to Publish** The authors have approved the paper and agree with its publication.

**Consent to Participate** No applicable.

**Competing Interests** The authors declare no competing interests.

## References


1. Tchounwou PB, Yedjou CG, Patlolla AK, Sutton DJ (2012) Heavy metal toxicity and the environment. EXS 101:133–164. https://doi.org/10.1007/978-3-7643-8340-4_6
2. Briffa J, Sinagra E, Blundell R (2020) Heavy metal pollution in the environment and their toxicological effects on humans. Heliyon 6. https://doi.org/10.1016/j.heliyon.2020.e04691
3. Wani AL, Ara A, Usmani JA (2015) Lead toxicity: A review. Interdiscip Toxicol 8:55–64. https://doi.org/10.1515/intox-2015-0009
4. Liu D, Shi Q, Liu C, Sun Q, Zeng X (2023) Effects of endocrine-disrupting heavy metals on human health. Toxics 11. https://doi.org/10.3390/TOXICS11040322
5. Buccolieri A, Buccolieri G, Dell'Atti A, Perrone MR, Turnone A (2006) Natural sources and heavy metals. Ann Chim 96:167–181. https://doi.org/10.1002/ADIC.200690017
6. Wuana RA, Okieimen FE (2011) Heavy metals in contaminated soils: A review of sources chemistry, risks and best available strategies for remediation. ISRN Ecol 2011:1–20. https://doi.org/10.5402/2011/402647
7. Gan Y, Huang X, Li S, Liu N, Li YC, Freidenreich A, Wang W, Wang R, Dai J (2019) Source quantification and potential risk of mercury, cadmium, arsenic, lead, and chromium in farmland soils of Yellow River Delta. J Clean Prod 221:98–107. https://doi.org/10.1016/J.JCLEPRO.2019.02.157
8. Kulkarni SJ (2020) Heavy metal pollution: Sources, effects, and control methods, hazard. Waste Manag Heal Risks 97–112. https://doi.org/10.2174/9789811454745120010008
9. Sharma N, Sodhi KK, Kumar M, Singh DK (2021) Heavy metal pollution: Insights into chromium eco-toxicity and recent advancement in its remediation. Environ Nanotechnol Monit Manag 15:100388. https://doi.org/10.1016/j.enmm.2020.100388
10. Yang Q, Li Z, Lu X, Duan Q, Huang L, Bi J (2018) A review of soil heavy metal pollution from industrial and agricultural regions in China: Pollution and risk assessment
11. Nagajyoti PC, Lee KD, Sreekanth TV (2010) Heavy metals, occurrence and toxicity for plants: A review. Environ Chem Lett 83(8):199–216. https://doi.org/10.1007/S10311-010-0297-8
12. Peter ALJ, Viraraghavan T (2005) Thallium: A review of public health and environmental concerns. Environ Int 31:493–501. https://doi.org/10.1016/j.envint.2004.09.003
13. Mohammed AS, Kapri A, Goel R (2011) Heavy metal pollution: Source, impact, and remedies. 1–28. https://doi.org/10.1007/978-94-007-1914-9_1
14. Fu Z, Xi S (2019) The effects of heavy metals on human metabolism. 30:167–176.https://doi.org/10.1080/15376516.2019.1701594
15. Reineke W, Schlömann M (2023) Heavy metals and other toxic inorganic ions. 331–348. https://doi.org/10.1007/978-3-662-66547-3_9
16. Kim JJ, Kim YS, Kumar V (2019) Heavy metal toxicity: An update of chelating therapeutic strategies. J Trace Elem Med Biol 54:226–231. https://doi.org/10.1016/j.jtemb.2019.05.003
17. Isangedighi IA, David GS (2019) Heavy metals contamination in fish: Effects on human health. J Aquat Sci Mar Biol 2
18. Giller KE, Witter E, McGrath SP (2009) Heavy metals and soil microbes. Soil Biol Biochem 41:2031–2037. https://doi.org/10.1016/J.SOILBIO.2009.04.026
19. Ramanujam J, Singh UP (2017) Copper indium gallium selenide based solar cells - A review. Energy Environ Sci 10:1306–1319. https://doi.org/10.1039/c7ee00826k
20. Kute AD, Gaikwad RP, Warkad IR, Gawande MB (2022) A review on the synthesis and applications of sustainable copper-based nanomaterials. Green Chem 24:3502–3573. https://doi.org/10.1039/D1GC04400A
21. Tuan WH, Lee SK (2014) Eutectic bonding of copper to ceramics for thermal dissipation applications – A review. J Eur Ceram Soc 34:4117–4130. https://doi.org/10.1016/J.JEURCERAMSOC.2014.07.011
22. Li X, Wang Y, Yin C, Yin Z (2020) Copper nanowires in recent electronic applications: Progress and perspectives. J Mater Chem C 8:849–872. https://doi.org/10.1039/C9TC04744A
23. Festa RA, Thiele DJ (2011) Copper: An essential metal in biology. Curr Biol 21. https://doi.org/10.1016/J.CUB.2011.09.040
24. Gunturu S, Dharmarajan TS (2020) Copper and zinc. Geriatr Gastroenterol 1–17. https://doi.org/10.1007/978-3-319-90761-1_25-1
25. Jomova K, Makova M, Alomar SY, Alwasel SH, Nepovimova E, Kuca K, Rhodes CJ, Valko M (2022) Essential metals in health and disease. Chem Biol Interact 367 https://doi.org/10.1016/J.CBI.2022.110173
26. Uauy R, Olivares M, Gonzalez M (1998) Essentiality of copper in humans. Am J Clin Nutr 67:952S–959S. https://doi.org/10.1093/ajcn/67.5.952S
27. Royer A, Sharman T (2021) Copper Toxicity, StatPearls Publishing. http://www.ncbi.nlm.nih.gov/pubmed/32491388. Accessed 17 April 2021
28. Uriu-Adams JY, Keen CL (2005) Copper, oxidative stress, and human health. Mol Aspects Med 26:268–298. https://doi.org/10.1016/J.MAM.2005.07.015
29. Brewer GJ (2012) Copper toxicity in Alzheimer's disease: Cognitive loss from ingestion of inorganic copper. J Trace Elem Med Biol 26:89–92. https://doi.org/10.1016/j.jtemb.2012.04.019
30. Barillo DJ, Marx DE (2014) Silver in medicine: A brief history BC 335 to present. Burns 40:S3–S8. https://doi.org/10.1016/J.BURNS.2014.09.009
31. Al-Saidi HM, Khan S (2022) A review on organic fluorimetric and colorimetric chemosensors for the detection of Ag(I) ions. Crit Rev Anal Chem. https://doi.org/10.1080/10408347.2022.2133561
32. Miyayama T, Arai Y, Hirano S (2016) Health effects of silver nanoparticles and silver ions. Biol Eff Fibrous Part Subst 137–147. https://doi.org/10.1007/978-4-431-55732-6_7
33. Hadrup N, Lam HR (2014) Oral toxicity of silver ions, silver nanoparticles and colloidal silver - A review. Regul Toxicol Pharmacol 68:1–7. https://doi.org/10.1016/j.yrtph.2013.11.002

34. Drake PL, Hazelwood KJ (2005) Exposure-related health effects of silver and silver compounds: A review. Ann Occup Hyg 49:575–585. https://doi.org/10.1093/ANNHYG/MEI019
35. Panyala NR, Peña-Méndez EM, Havel J (2008) Silver or silver nanoparticles: A hazardous threat to the environment and human health? J Appl Biomed 6:117–129. www.zsf.jcu.cz/jab. Accessed 18 May 2021
36. Qu H, Mudalige TK, Linder SW (2016) Capillary electrophoresis coupled with inductively coupled mass spectrometry as an alternative to cloud point extraction based methods for rapid quantification of silver ions and surface coated silver nanoparticles. J Chromatogr A 1429:348–353. https://doi.org/10.1016/J.CHROMA.2015.12.033
37. Tung NH, Chikae M, Ukita Y, Viet PH, Takamura Y (2012) Sensing technique of silver nanoparticles as labels for immunoassay using liquid electrode plasma atomic emission spectrometry. Anal Chem 84:1210–1213. https://doi.org/10.1021/AC202782B/SUPPL_FILE/AC202782B_SI_001.PDF
38. Mohammadi SZ, Afzali D, Taher MA, Baghelani YM (2009) Ligandless dispersive liquid–liquid microextraction for the separation of trace amounts of silver ions in water samples and flame atomic absorption spectrometry determination. Talanta 80:875–879. https://doi.org/10.1016/J.TALANTA.2009.08.009
39. Wang S, Forzani ES, Tao N (2007) Detection of heavy metal ions in water by high-resolution surface plasmon resonance spectroscopy combined with anodic stripping voltammetry. Anal Chem 79:4427–4432. https://doi.org/10.1021/AC0621773/SUPPL_FILE/AC0621773SI20070226_071019.PDF
40. Otero-Romaní J, Moreda-Piñeiro A, Bermejo-Barrera P, Martin-Esteban A (2009) Inductively coupled plasma–optical emission spectrometry/mass spectrometry for the determination of Cu, Ni, Pb and Zn in seawater after ionic imprinted polymer based solid phase extraction. Talanta 79:723–729. https://doi.org/10.1016/J.TALANTA.2009.04.066
41. Ghaedi M, Mortazavi K, Montazerozohori M, Shokrollahi A, Soylak M (2013) Flame atomic absorption spectrometric (FAAS) determination of copper, iron and zinc in food samples after solid-phase extraction on Schiff base-modified duolite XAD 761. Mater Sci Eng C 33:2338–2344. https://doi.org/10.1016/J.MSEC.2013.01.062
42. Sardans J, Montes F, Peñuelas J (2010) Determination of As, Cd, Cu, Hg and Pb in biological samples by modern electrothermal atomic absorption spectrometry, Spectrochim. Acta - Part B Spectrosc 65:97–112. https://doi.org/10.1016/J.SAB.2009.11.009
43. Yang GY, Li Z, Shi HL, Wang J (2005) Study on the determination of heavy-metal ions in tobacco and tobacco additives by microwave digestion and HPLC with PAD detection. J Anal Chem 605(60):480–485. https://doi.org/10.1007/S10809-005-0123-9
44. Stojanović Z, Koudelkova Z, Sedlackova E, Hynek D, Richtera L, Adam V (2018) Determination of chromium(VI) by anodic stripping voltammetry using a silver-plated glassy carbon electrode. Anal Methods 10:2917–2923. https://doi.org/10.1039/C8AY01047A
45. Alhamami MAM, Algethami JS, Khan S (2023) A review on thiazole based colorimetric and fluorimetric chemosensors for the detection of heavy metal ions. Crit Rev Anal Chem. https://doi.org/10.1080/10408347.2023.2197073
46. Algethami JS (2022) A review on recent progress in organic fluorimetric and colorimetric chemosensors for the detection of Cr 3+/6+ Ions. Crit Rev Anal Chem 1–21. https://doi.org/10.1080/10408347.2022.2082242
47. Khan S, Chen X, Almahri A, Allehyani ES, Alhumaydhi FA, Ibrahim MM, Ali S (2021) Recent developments in fluorescent and colorimetric chemosensors based on schiff bases for metallic cations detection: A review. J Environ Chem Eng 9. https://doi.org/10.1016/J.JECE.2021.106381
48. Berhanu AL, Gaurav I, Mohiuddin AK, Malik JS, Aulakh V, Kumar KH, Kim A (2019) Review of the applications of Schiff bases as optical chemical sensors. TrAC - Trends Anal Chem 116:74–91. https://doi.org/10.1016/j.trac.2019.04.025
49. Hussain Z, Yousif E, Ahmed A, Altaie A (2014) Synthesis and characterization of Schiff's bases of sulfamethoxazole. Org Med Chem Lett 41(4):1–4. https://doi.org/10.1186/2191-2858-4-1
50. Kaya I, Solak E, Kamaci M (2021) Synthesis and multicolor, photophysical, thermal, and conductivity properties of poly(imine)s. J Taiwan Inst Chem Eng 123:328–337. https://doi.org/10.1016/J.JTICE.2021.05.010
51. Saydam S (2007) Synthesis and characterisation of the new thiazole schiff base 2-(2-hydroxy)naphthylideneamino-benzothiazole and its complexes with Co(II), Cu(II), AND Ni(II) ions. 32:437–447. https://doi.org/10.1081/SIM-120003787
52. Hassan AM, Said AO, Heakal BH, Younis A, Aboulthana WM, Mady MF (2022) Green synthesis, characterization, antimicrobial and anticancer screening of new metal complexes incorporating schiff base, ACS. Omega 7:32418–32431. https://doi.org/10.1021/ACSOMEGA.2C03911/ASSET/IMAGES/LARGE/AO2C03911_0009.JPEG
53. Al-Harbi S, Al-Harbi SA, Bashandy MS, Al-Saidi HM, Emara AAA, El-Gilil SMA (2016) Spectroscopic properties, anti-colon cancer, antimicrobial and molecular docking studies of silver(I), manganese(II), cobalt(II) and nickel(II) complexes for 2-amino-4-phenylthiazole derivative. Eur J Chem 7:421–430. https://doi.org/10.5155/eurjchem.7.4.421-430.1490
54. Mergu N, Gupta VK (2015) A novel colorimetric detection probe for copper(II) ions based on a Schiff base. Sens Actuators B Chem 210:408–417. https://doi.org/10.1016/J.SNB.2014.12.130
55. Zhu Wan-Yu, Liu Kai, Zhang Xuan (2023) A benzimidazole-derived fluorescent chemosensor for Cu( ii )-selective turn-off and Zn( ii )-selective ratiometric turn-on detection in aqueous solutions. Sens Diagnos 2:665–675. https://doi.org/10.1039/D3SD00020F
56. Wang L, Bing Q, Li J, Wang G (2018) A new "ON-OFF" fluorescent and colorimetric chemosensor based on 1,3,4-oxadiazole derivative for the detection of Cu2+ ions. J Photochem Photobiol A Chem 360:86–94. https://doi.org/10.1016/J.JPHOTOCHEM.2018.04.015
57. Affrose A, Parveen SDS, Kumar BS, Pitchumani K (2015) Selective sensing of silver ion using berberine, a naturally occurring plant alkaloid. Sens Actuators B Chem 206:170–175. https://doi.org/10.1016/J.SNB.2014.09.042
58. Bhuvanesh N, Suresh S, Kumar PR, Mothi EM, Kannan K, Kannan VR, Nandhakumar R (2018) Small molecule "turn on" fluorescent probe for silver ion and application to bioimaging. J Photochem Photobiol A Chem 360:6–12. https://doi.org/10.1016/J.JPHOTOCHEM.2018.04.027
59. Rout K, Manna AK, Sahu M, Mondal J, Singh SK, Patra GK (2019) Triazole-based novel bis Schiff base colorimetric and fluorescent turn-on dual chemosensor for Cu 2+ and Pb 2+: Application to living cell imaging and molecular logic gates. RSC Adv 9:25919–25931. https://doi.org/10.1039/C9RA03341F
60. Liu Y, Jiang B, Zhao L, Zhao L, Wang Q, Wang C, Xu B (2021) A dansyl-based fluorescent probe for sensing Cu2+ in aqueous solution. Spectrochim Acta Part A Mol Biomol Spectrosc 261. https://doi.org/10.1016/J.SAA.2021.120009
61. Wu YC, Jiang K, Luo SH, Cao L, Wu HQ, Wang ZY (2019) Novel dual-functional fluorescent sensors based on bis(5,6-dimethylbenzimidazole) derivatives for distinguishing of Ag+ and Fe3+ in semi-aqueous medium. Spectrochim Acta Part A Mol Biomol Spectrosc 206:632–641. https://doi.org/10.1016/J.SAA.2018.05.069
62. Zhang Y, Wang D, Sun C, Feng H, Zhao D, Bi Y (2017) A simple 2,6-diphenylpyridine-based fluorescence "turn-on" chemosensor

for Ag+ with a high luminescence quantum yield. Dye Pigment 141:202–208. https://doi.org/10.1016/J.DYEPIG.2017.02.028
63. Karkosik A, Moro AJ (2022) An NIR emissive donor-π-acceptor dicyanomethylene-4h-pyran derivative as a fluorescent chemosensor system towards copper (II) detection. Chemosensors 10:343. https://doi.org/10.3390/CHEMOSENSORS10080343/S1
64. Lin Q, Yang Q, Sun B, Wei T, Zhang Y (2014) A novel highly selective "Turn-On" fluorescence sensor for silver ions based on Schiff base. Chin J Chem 32:1255–1258. https://doi.org/10.1002/cjoc.201400601
65. Yang JY, Gao WY, Wang JH, Dong ZM, Wang Y, Shuang SM (2023) A new NBD-based probe for specific colorimetric and turn-on fluorescence sensing of Cu2+ and bio-imaging applications. J Lumin 254. https://doi.org/10.1016/J.JLUMIN.2022.119549
66. Zhang S, Wu X, Niu Q, Guo Z, Li T, Liu H (2005) Highly selective and sensitive colorimetric and fluorescent chemosensor for rapid detection of Ag +, Cu 2+ and Hg 2+ based on a simple Schiff base. Springer 27:729–737. https://doi.org/10.1007/s10895-016-2005-y
67. Liu L, Liu X, Guo C, Fang M, Li C, Zhu W (2021) Carbazole-based dual-functional chemosensor: Colorimetric sensor for Co2+ and fluorescent sensor for Cu2+ and its application. J Chin Chem Soc 68:2368–2377. https://doi.org/10.1002/JCCS.202100343
68. Tümay SO (2021) A novel selective "Turn-On" fluorescent chemosensor based on thiophene appended cyclotriphosphazene Schiff base for detection of Ag+ ions. Chem Select 6:10561–10572. https://doi.org/10.1002/SLCT.202102052
69. Khan S, Muhammad M, Kamran AW, Al-Saidi HM, Alharthi SS, Algethami JS (2023) An ultrasensitive colorimetric and fluorescent "turn-on" chemosensor based on Schiff base for the detection of Cu2+ in the aqueous medium. Environ Monit Assess 195. https://doi.org/10.1007/S10661-023-11260-3
70. Chen C, Liu H, Zhang B, Wang Y, Cai K, Tan Y, Gao C, Liu H, Tan C, Jiang Y (2016) A simple benzimidazole quinoline-conjugate fluorescent chemosensor for highly selective detection of Ag+. Tetrahedron 72:3980–3985. https://doi.org/10.1016/J.TET.2016.05.020
71. Slassi S, Aarjane M, Amine A (2021) A novel imidazole-derived Schiff base as selective and sensitive colorimetric chemosensor for fluorescent detection of Cu2+ in methanol with mixed aqueous medium. Appl Organomet Chem 35. https://doi.org/10.1002/AOC.6408
72. Wang L, Zhang C, He H, Zhu H, Guo W, Zhou S, Wang S, Zhao JR, Zhang J (2020) Cellulose-based colorimetric sensor with N, S sites for Ag+ detection. Int J Biol Macromol 163:593–602. https://doi.org/10.1016/j.ijbiomac.2020.07.018
73. Dongare PR, Gore AH, Kolekar GB, Ajalkar BD (2020) A Phenazine based colorimetric and fluorescent chemosensor for sequential detection of Ag+ and I− in aqueous media. Luminescence 35:231–242. https://doi.org/10.1002/BIO.3718
74. Rahimi H, Hosseinzadeh R, Tajbakhsh M (2021) A new and efficient pyridine-2,6-dicarboxamide-based fluorescent and colorimetric chemosensor for sensitive and selective recognition of Pb2+ and Cu2+. J Photochem Photobiol A Chem 407. https://doi.org/10.1016/J.JPHOTOCHEM.2020.113049
75. Nagarajan R, Ryoo HI, Vanjare BD, Choi NG, Lee KH (2021) Novel phenylalanine derivative-based turn-off fluorescent chemosensor for selective Cu2+ detection in physiological pH. J Photochem Photobiol A Chem 418:113435. https://doi.org/10.1016/J.JPHOTOCHEM.2021.113435
76. Anand T, Sivaraman G, Anandh P, Chellappa D, Govindarajan S (2014) Colorimetric and turn-on fluorescence detection of Ag(I) ion. Tetrahedron Lett 55:671–675. https://doi.org/10.1016/J.TETLET.2013.11.104
77. Cui W, Wang L, Xiang G, Zhou L, An X, Cao D (2015) A colorimetric and fluorescence "turn-off" chemosensor for the detection of silver ion based on a conjugated polymer containing 2,3-di(pyridin-2-yl)quinoxaline. Sensors Actuators B Chem 207:281–290. https://doi.org/10.1016/J.SNB.2014.10.072
78. Mani KS, Rajamanikandan R, Murugesapandian B, Shankar R, Sivaraman G, Ilanchelian M, Rajendran SP (2019) Coumarin based hydrazone as an ICT-based fluorescence chemosensor for the detection of Cu2+ ions and the application in HeLa cells. Spectrochim Acta Part A Mol Biomol Spectrosc 214:170–176. https://doi.org/10.1016/J.SAA.2019.02.020
79. Tharmaraj V, Devi S, Pitchumani K (2012) An intramolecular charge transfer (ICT) based chemosensor for silver ion using 4-methoxy-N-((thiophen-2-yl)methyl)benzenamine. Analyst 137:5320–5324. https://doi.org/10.1039/C2AN35721F
80. Warrier SB, Kharkar PS (2018) A coumarin based chemosensor for selective determination of Cu (II) ions based on fluorescence quenching. J Lumin 199:407–415. https://doi.org/10.1016/J.JLUMIN.2018.03.073
81. Velmurugan K, Suresh S, Santhoshkumar S, Saranya M, Nandhakumar R (2016) A simple chalcone-based ratiometric chemosensor for silver ion. Luminescence 31:722–727. https://doi.org/10.1002/BIO.3016
82. Wang J, Niu Q, Wei T, Li T, Hu T, Chen J, Qin X, Yang Q, Yang L (2020) Novel phenothiazine-based fast-responsive colori/fluorimetric sensor for highly sensitive, selective and reversible detection of Cu2+ in real water samples and its application as an efficient solid-state sensor. Microchem J 157. https://doi.org/10.1016/J.MICROC.2020.104990
83. Bhuvanesh N, Suresh S, Prabhu J, Kannan K, Kannan VR, Nandhakumar R (2018) Ratiometric fluorescent chemosensor for silver ion and its bacterial cell imaging. Opt Mater (Amst) 82:123–129. https://doi.org/10.1016/J.OPTMAT.2018.05.053
84. Zhang Y, Li H, Pu S (2020) A colorimetric and fluorescent probe based on diarylethene for dual recognition of Cu2+ and CO32- and its application. J Photoch Photobiol A Chem 400. https://doi.org/10.1016/J.JPHOTOCHEM.2020.112721
85. Zhao H, Ding H, Kang H, Fan C, Liu G, Pu S (2019) A solvent-dependent chemosensor for fluorimetric detection of Hg 2+ and colorimetric detection of Cu 2+ based on a new diarylethene with a rhodamine B unit. RSC Adv 9:42155–42162. https://doi.org/10.1039/C9RA08557B
86. Li WT, Wu GY, Qu WJ, Li Q, Lou JC, Lin Q, Yao H, Zhang YM, Wei TB (2017) A colorimetric and reversible fluorescent chemosensor for Ag+ in aqueous solution and its application in IMPLICATION logic gate. Sens Actuators B Chem 239:671–678. https://doi.org/10.1016/J.SNB.2016.08.016
87. Bao Z, Qin C, Wang JJ, Sun J, Dai L, Chen G, Mei F (2018) A sensitive and selective probe for visual detection of Cu2+ based on 1, 8-naphthalimidederivative. Sens Actuators B Chem 265:234–241. https://doi.org/10.1016/J.SNB.2018.03.050